ASTRONOMY & ASTROPHYSICS
SUPPLEMENT SERIES

Astron. Astrophys. Suppl. Ser. **101,** 109-126 (1993)

Monitoring OH/IR stars at the Galactic centre with the VLA

H.J. Van Langevelde[1], A.M. Janssens[1], W.M. Goss[2], H.J. Habing[1] and A. Winnberg[3]

[1] Sterrewacht Leiden, P.O. Box 9513, 2300 RA Leiden, the Netherlands
[2] N.R.A.O., P.O. Box 0, Socorro, NM 87801, U.S.A.
[3] Onsala Space Observatory, S-43900, Sweden

Received November 17, 1992; accepted January 18, 1993

Abstract. — We present data on the variability of OH/IR stars at the Galactic centre. The observations were carried out with the VLA at 1612 MHz at 20 separate epochs over a period of three years. For each epoch 37 circumstellar OH maser sources were observed. In this paper the unique data reduction procedures for this project are described. We present "light curves" for the stars in the sample to which a periodic curve is fitted. The resulting periods are compared with those found for OH/IR stars found in various other parts of the Galaxy. For the "best" stars in our sample the phase lag between the blue and red-shifted part of the spectrum can be determined.

Key words: stars: OH/IR — interferometry — galaxy (the): center of — masers — stars: variable

1. Introduction

1.1. *The variability of OH/IR stars*

During the last two decades a great deal of effort has been put into monitoring the variability of OH/IR stars at 1612 MHz. These observations were always carried out with single dish telescopes. One of the main goals of these extensive observing programs has been the measurement of the phase lags in OH/IR stars, which is the time delay between the variations of the blue and red-shifted peak in the OH spectrum (Van Langevelde et al. 1990; Herman & Habing 1985a). This phase lag yields a direct measurement of the radius of the circumstellar OH shell and can be combined with a measurement of the angular size to obtain the distance to the object (see Herman & Habing 1985b or Cohen 1989, for a review on OH/IR stars).

Apart from this interest in phase lags, various authors have discussed the periods of Asymptotic Giant Branch (AGB) stars in terms of the evolution of the underlying star (Herman & Habing 1985a; Engels et al. 1983; Wood 1989; Van der Veen & Habing 1990; Whitelock et al. 1991). OH/IR stars are objects on the AGB, giant stars that suffer high mass loss. Like Miras these stars show strong variability in their total luminosity. Because the OH maser is (indirectly) pumped by the stellar radiation the same variability is detected in the OH. Periods in the range 400 - 2000 days are typically found.

Send offprint requests to: H.J. Van Langevelde

1.2. *OH/IR stars at the Galactic centre*

A large number of OH/IR stars in the Galactic centre are known (Lindqvist et al. 1992a). In six VLA[1] primary beams (30′ across) near SgrA* 134 OH/IR stars were discovered with flux densities above 100 mJy. The aim of the survey was to study the kinematics of these stars around the Galactic centre (Lindqvist et al. 1992b). These objects can also be used to obtain a direct and independent measurement of the distance to the Galactic centre. Monitoring OH/IR stars at the Galactic centre, however, poses some special difficulties.

Sensitivity is not the major consideration; even at the Galactic centre OH/IR stars are still bright enough to give reasonable signal to noise ratios with large single dish telescopes. The problems with single dish observations are confusion amongst the OH/IR stars and the bright emission of the Galactic centre, which also shows strong absorption at 1612 MHz. These problems must be solved; to obtain accurate variability curves for the OH sources we need uncontaminated spectra of every OH/IR star.

Therefore the VLA was used to monitor the variability of the OH masers. In one single pointing we can distinguish many OH/IR stars over the primary beam. In this way a phase lag for several sources can be obtained. Combined with angular size determinations, several in-

[1] The Very Large Array (VLA) is operated by the National Radio Astronomy Observatory under cooperative agreement with the National Science Foundation

dependent measurements of the distance to the Galactic centre could in principle be obtained.

Unfortunately recent results on angular broadening by interstellar scattering (Van Langevelde & Diamond 1991, Van Langevelde et al. 1992) show that the intrinsic angular sizes of these OH/IR stars at the Galactic centre can not be measured, thus making the distance determination impossible. But the data on the variability of OH/IR stars can also be used to study stellar evolution. Determining the periods of these stars will give information on stellar ages at the centre of the Galaxy especially when combined with bolometric luminosities that can be obtained by infrared photometry (Blommaert et al. 1993).

1.3. *Outline of this paper*

We will first discuss the sample. Next the parameters of the observations are presented, followed by a discussion of the reduction techniques with special emphasis on the uncertainties in the flux density determinations. Periods and phase lags of the stars are presented.

We point out that the raw visibility data set obtained is large ($\approx$ 20 GByte). Therefore it was not always possible to apply the most optimum data reduction procedure.

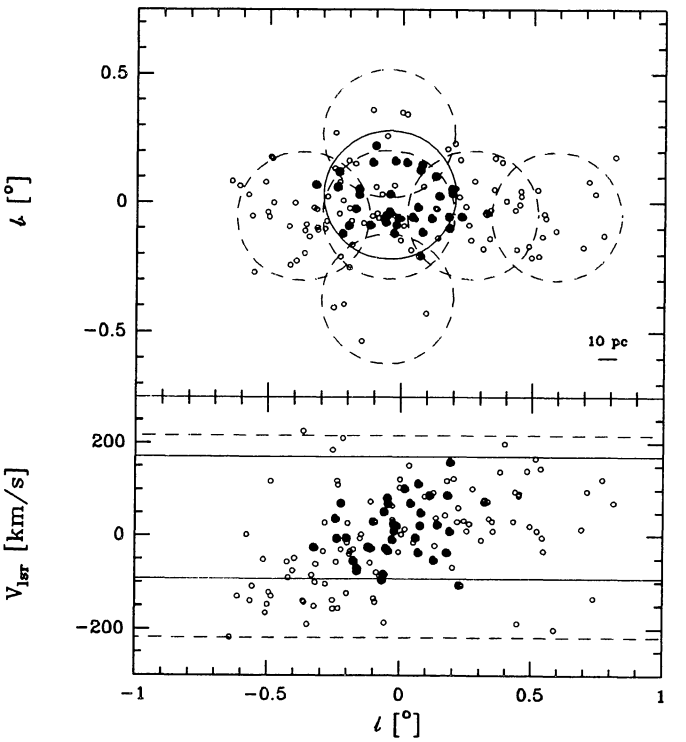

Fig. 1. OH/IR stars from the Lindqvist et al. (1992a) sample (open symbols) and the sample selected for the monitor program

2. The sample

The observations presented here were made in a field centred close to SgrA. The pointing position was chosen to have as many bright OH masers as possible within the primary beam in order to get an accurate distance determination. For the measurement of the phase lag sufficient spectral resolution was required. We used 256 channels, each 6.3 kHz wide (see Table 1).

In the field of view (in RA, Dec., and frequency) many OH/IR stars from the Lindqvist et al. (1992a) catalogue are present. We decided to consider in our study of variability OH/IR stars for which we have sufficient sensitivity to detect variability, considering the flux density that Lindqvist et al. (1992a) list; all sources above 210 mJy (for the field centre) were selected. This is seven times the noise in the monitor observations of least sensitivity. We have taken into account the attenuation of the primary beam when defining the sample; 37 objects then meet the criteria. In Fig. 1 we show the stars of the Lindqvist et al. (1992a) sample and our selection from it (see also Tables 3, 4 and 5). Spectra of these objects can be found in Lindqvist et al. (1992a).

Because these objects often vary in flux density by more than a factor of two, some of the stars that are not included in the sample might become bright enough during the monitoring that useful measurements can be made. Some previously unknown sources may even "appear" during the observations. However, it is unlikely that we could derive periods and phase lags for these stars. Searching for "new" OH/IR sources is best done by concatenating all the data sets together, instead of searching every single epoch separately. We should be aware that the sample under consideration is not complete. The bias towards strong OH sources is even worse when the properties of variability will be discussed; only for strong sources the variations can be accurately monitored.

3. The observations and data reduction strategy

3.1. *Parameters of the observations*

The observations took place between January 1988 and January 1991. In principle, once every seven weeks the VLA observed this field for two hours. This strategy implies that the VLA was used in different configurations from epoch to epoch. With the pointing position chosen, SgrA is in the primary beam. SgrA* is 4.7 arcmin away from the field centre. As an extra complication there is also extended OH 1612 MHz absorption observed in the direction of SgrA at several velocities (e.g. Habing et al. 1983). In view of the enormous amount of continuum emission and given the extended nature of the absorption, we never observed when the VLA was in D configuration. In D array also serious problems with confusion among the OH masers would occur.

Table 1. Parameters for all the observations

field centre (1950)	$17^h42^m12^s.60$ $-28°56'18''.00$
Galactic coordinates	359.9548 0.0321
Primary beam (FWHM)	27.6 arcmin
v_{lsr} of centre of band	+40 km/s
observing frequency	1612.23101 MHz
bandwidth	1.56625 MHz or 290.64 km/s
resolution	6.10 kHz or 1.14 km/s

Every observation was carried out with the same observing parameters, listed in Table 1. Before August 1988 observations were performed in the right handed polarisation (RR), subsequent improvements in the on-line computer at the VLA made it possible to use LL and RR simultaneously. In all cases the data were recorded at 20 second intervals, though this time resolution was only preserved for the reduction of A-array data. In other configurations the data were averaged to 1 minute. The trade off is between avoiding time smearing and the size of the data sets.

Table 2. Observing dates and remarks on individual cases. Col. 4 lists the noise in a single channel. Several observations were scheduled for transition configurations of the VLA

Obs. date (Time in UT)		Julian date	conf.	noise [mJy]	$S_{1748-253}$ [Jy]	±
29/ 2/88	13 : 37	7221.07	BC	31	1.109	0.005
7/ 4/88	12 : 13	7259.01	CD	34	1.200	0.090
22/ 5/88	8 : 30	7303.85	CD	24	1.132	0.004
17/10/88	22 : 25	7452.43	A	14	1.200	0.014
22/11/88	23 : 00	7488.46	A	14	no 3C286	
27/12/88	20 : 15	7523.34	AB	15	–	–
9/ 2/89	13 : 52	7567.08	AB	60	1.130	0.018
1/ 4/89	10 : 31	7617.94	B	12	1.170	0.019
14/ 5/89	10 : 41	7660.95	BC	20	1.145	0.007
2/ 7/89	3 : 30	7709.65	C	33	1.170	0.050
31/ 8/89	4 : 04	7769.67	BC	23	1.123	0.008
8/ 2/90	13 : 58	7931.08	AD	16	no 3C286	
1/ 3/90	13 : 05	7952.04	A	14	1.154	0.009
27/ 4/90	11 : 50	8008.99	A	13	1.160	0.097
5/ 6/90	8 : 17	8047.85	AB	14	1.138	0.006
26/ 7/90	4 : 26	8098.68	B	14	1.078	0.020
17/ 9/90	1 : 27	8151.56	B	13	1.164	0.007
18/12/90	18 : 52	8244.29	C	20	1.120	0.050
26/ 1/91	17 : 50	8283.24	C	19	1.177	0.006

3.2. *Calibration*

All data were calibrated and further processed using the AIPS package.

During each two hour observing period 20 minutes were spent on calibration. 3C286 was observed at the beginning of the observations and 1748−253 (almost 4° away from the Galactic centre, ≈ 1.17 Jy at 18 cm) was observed every 25 minutes as a secondary phase and amplitude calibrator. The derived values for the flux density of 1748−253 were investigated for systematic effects with resolution. No effect with configuration was found; there does seem to be some indication of variability of 1748−253 (Table 2). In some cases (especially in A-array) a single iteration of self-calibration for phase was required. The amplitude gain of the telescopes was not allowed to be adjusted in the self-calibration scheme, because for the monitoring the flux density scale must be derived from the calibrators.

The source 3C286 was also used as a bandpass calibrator. In the calculations the bandpass was always assumed to be constant during the two hour observations. For some observations 1748−253 was used for bandpass calibration. This will lead to a higher uncertainty in the calibration of each channel. For two epochs the observations on 3C286 were lost due to technical failures. These observations were calibrated assuming a flux density of 1.15 Jy for 1748−253. For all cases the resulting errors in the final flux scale were estimated and used in the analysis of the OH/IR star variability.

Three observations were clearly affected by interference. For the observations in C array at 18/12/90 most of the short baselines had to be deleted, likely because of interference from the sun, 5.6 degrees away. The GLONASS satellites were the source of trouble for the observations on 1/3/90 and 9/2/89. The data from this last epoch was not used in the analysis of a number of sources.

3.3. *Measuring the OH flux densities*

To be able to measure the OH spectra accurately the strong continuum emission from the Galactic centre must be subtracted. Because of the specific conditions of these observations, we have applied visibility based continuum subtraction, (Van Langevelde & Cotton 1990, Cornwell et al. 1992). The case described here is very well suited for visibility based subtraction because the relative bandwidth is small; the spectrum of a single OH/IR star usually spans less than 250 kHz. After continuum subtraction, the AIPS task MX was used to create small cubes centred on the position and velocity of each OH maser source. In this process only data from baselines longer than 3 kλ were used; the shorter baselines show extended 1612 MHz absorption. The maps were made using natural weighting. Because the images usually contain just a single point source cleaning is easy. For some sources special caution

had to be taken because sidelobes caused by near sources interfere in the small images.

Finally the standard correction for primary beam attenuation is applied. The polynomial description of the beam in the AIPS task PBCOR can not correct fully for the effects of varying response over the field of view. We are especially concerned whether the correction can be taken constant for observations at different epochs. Two factors should be considered here.

1. First, pointing errors of individual telescopes cause changes in the primary beam response. This effect can be estimated from the first derivative of the shape of the primary beam and the rms pointing error. Typical values are 2% at the factor two attenuation (14′ radius).
2. Another effect is caused by the fact that the receivers are off-axis and at different positions for LL and RR. Because the the telescopes of the VLA are alt-az mounted the resulting beam is not constant from epoch to epoch. The effect on the total intensity will be small (typical numbers are 0.1% at the edge of the primary beam, Thomson 1976), but can be larger for the observations done with single polarisation.

Thus the uncertainty in the primary beam response is a factor that can limit the accuracy of the monitor capabilities. We have estimated the errors involved to be used in further analysis.

From the images the flux density of the sources was determined. There are several effects in this step that contribute to the final error. Intrinsically stars at the distance to the Galactic centre are expected to appear as point sources, even in the A-array. However, instrumental effects make the image appear slightly broadened. For instance smearing by time averaging could cause this. This effect scales linearly with baseline length and will most serious in A-array. For the A-array data (and AB transition as well) the 20 second integration time was kept, for all other configurations it was averaged to 60 seconds. In this way the time smearing in A and B array at the edge of the beam is 1.3 times the beamsize, for C-array data it is only 0.4. Furthermore there is some smearing due to the effect of non coplanar baselines (Cornwell & Perley 1992). To map a small patch around a source away from the phase centre the AIPS task MX makes a first order approximation of the change in phase for the new map centre, instead of recalculating phase and u, v, w coordinates. This results in a peculiar smearing of the image, introducing increasing problems away from the phase centre. Furthermore it has been shown recently that interstellar scattering for several OH/IR stars may cause angular broadening as big as several arcseconds (Diamond et al. 1993).

These effects result in some extent of the images of the point-sources. To monitor our sources we therefore measure the integrated flux density in the maps. This proved a good way to obtain the flux density from the smeared images without introducing a bias. When we had to determine the flux density in a large number of maps across the spectrum, we assumed that this smearing is constant in all channels. So the integrated flux density in each channel was estimated from the peak flux density and the smearing in the channel with best signal to noise ratio.

4. Results

The positions and velocities of all masers from epoch to epoch were checked. No systematic changes were found in position or in velocity; all masers were observed every epoch at the same position within the errors (typically 1″) and in the same velocity channels. The improved positions of the sources are listed in Table 3, 4 and 5.

Considerable effort has been made to estimate the error in the flux density determination. This is a crucial step in the measurements of variability, periods and phase lags. The effects of flux calibration, bandpass calibration, pointing errors and primary beam response and the final determination from the images have been estimated as described above. Typically it is found that for sources brighter than 1 Jy (in the inner part of the beam) the limit is due to calibration (i.e. including primary beam), while for weaker sources it is the thermal noise. When doing the phase lag measurements we should be careful how much of these effects correlate across the spectrum. The inaccuracies introduced by the primary beam and the total calibration are systematic across the spectrum and may introduce systematic errors.

In Figs. 2, 3 and 4 the data for all of the sources from the sample are presented with a fitted light curve when possible (the fitting procedure will be described in Sect. 4.1). The results of the fits are categorised into three groups: (1) contains objects for which a period could be determined safely, group (2) contains objects that generally show variability but for which no period can be estimated unambiguously. Group (3) consists of objects that show no well-behaved variability. It is clear that group (2) contains predominantly weak objects. All bright objects ($F_i > 1.2$ Jy) are clearly variable or non−variable.

For each star the flux density in a single channel is shown for the red and blue-shifted peak of each observation and of the original detections in Lindqvist et al. (1992a). The error bars in the plots are estimated from a combination of uncertainties, as discussed above, i.e. calibration, primary beam correction, thermal noise and the fitting procedure of the profiles in images. Apart from displaying the data points at their true epoch (indicated by error bars), we also show each observation at every cycle at the appropriate relative phase (indicated by the small symbols).

For several sources only one of the two spectral peaks could be monitored. For OH 0.225−0.055, OH 359.838+0.052 and OH 359.932−0.063 the second peak was outside of the observing band. For OH 0.190+0.036 the two curves in the figure fall on top of each other. For all other sources for which a single peak is displayed the second one was too weak. The source OH 0.180−0.098 is missing from all tables and figures although it was in the original sample. In a few cases this source was detected, but its flux density was more than a factor of two less than the value determined by Lindqvist et al. (1992a). A number of sources are clearly not variable, although they are bright enough to obtain good signal to noise data. Especially OH 359.952−0.036 and OH 359.938−0.077 are in this category.

4.1. *Periods*

To determine the periods of the variable objects a model fit approach was adopted. Following Herman & Habing 1985a, an asymmetric cosine curve is chosen to describe the fluctuations of the logarithm of the flux density. This model describes the variation of the spectrum $S_\nu(t)$ with the same period, amplitude and phase for the entire spectrum and thus ignores the presence of a phase lag, but this is a very small effect:

$$\log S_\nu(t_i) = a_\nu + b\cos(2\pi\phi(t_i)), \qquad (1)$$

where

$$\phi(t) = \begin{cases} \frac{\varphi}{2f} & \text{when } 0 \le \varphi < f, \\ \frac{\varphi-1}{2(1-f)} + 1 & \text{when } f \le \varphi < 1, \end{cases}$$

and

$$\varphi = (t_i - t_0)/P.$$

In this formulation f is the asymmetry parameter. For these kind of objects $f \le 0.5$ is generally found (Herman & Habing 1985a). For $f = 0.5$ the asymmetric light curves is equivalent to the cosine. To fit a, b, P, T_0 and f with a non-linear least squares algorothm can be quite an unstable procedure, because a periodic function is to be fitted with only a few points of limited signal to noise. We have adopted a linearized fit in which we use $\hat{P}$ as a parameter. With $f = 0.5$ for the initial search we can write

$$\log S_\nu(t_i) = x_1 + x_2\cos\left(\frac{t_i 2\pi}{\hat{P}}\right) + x_3\sin\left(\frac{t_i 2\pi}{\hat{P}}\right), \qquad (2)$$

where

$$x_1 = a$$
$$x_2 = b\cos\left(\frac{t_0 2\pi}{\hat{P}}\right)$$
$$x_3 = b\sin\left(\frac{t_0 2\pi}{\hat{P}}\right)$$

In this way a linear fit for the x_i for each possibility $\hat{P}$ can be made. In a plot of χ^2 with $\hat{P}$ the global minimum for the period of the star can be found. An example of such a figure of $\chi^2 - \hat{P}$ is presented in Fig. 5. This method of finding the period has some advantages. First, a non-linear fitting algorithm is avoided. Second, the $\chi^2 - \hat{P}$ diagram immediately shows when there are other possible periods to fit the data. So when there is more than a single minimum of χ^2 this can be immediately recognised. Such a situation can easily occur, because the limited number of observations can impose a period on the data. After a model to the data has been found in this way, a non-linear least squares fit can be used to determine f. For this fitting procedure good initial estimates of the parameters are already available.

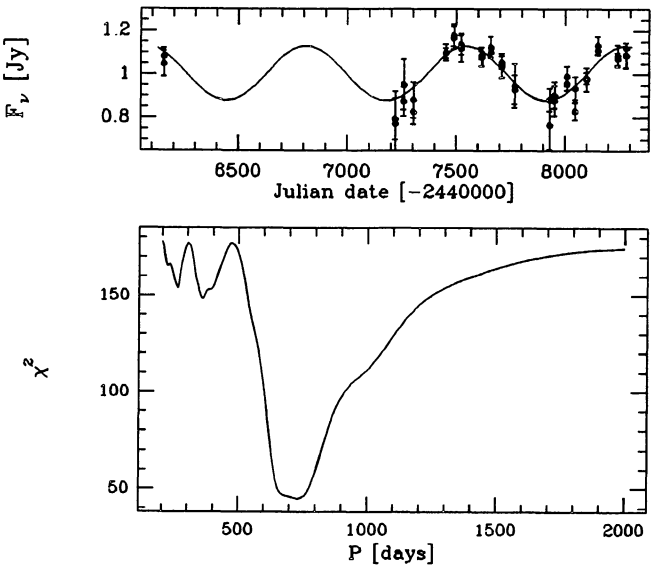

Fig. 5. A plot of χ^2 with $\hat{P}$ for OH 0.142+0.026

In the process to model the data the validity of the error estimates can be checked. The estimated observational errors should be sufficient to explain the residuals of the fit if the model is an adequate description of the observations. It was found that generally the uncertainties in the data can explain the deviations from the fit. In several cases the deviations are larger; we attribute this to intrinsic deviations from the smooth model, in particular the variations may not repeat exactly from cycle to cycle. In Tables 3, 4 and 5 the periods and other parameters of the fits are presented. Where possible, the results are obtained from a simultaneous fit of the blue and red-shifted peak. The errors given here are the formal errors from the uncertainties in the observations. They do not reflect the quality of the fit.

4.2. *Phase lags*

The same data set can be used to measure phase lags for the stars in the current sample. This can just be done for those objects for which the variability can be followed with reasonable accuracy of *both* the blue and red-shifted peak in the spectrum. A small subsample of five objects is defined for which these conditions are satisfied. For these stars the full spectrum at each epoch was used, because every spectral channel may contribute to the measurement of the phase lag. The algorithm that was used is described in detail by Van Langevelde et al. (1990).

Several of the considerations on error budget are of great importance when it comes to measuring phase lags. First a good knowledge of the uncertainty in every data point is essential in the Monte Carlo method described in Van Langevelde et al. (1990), both to weight the combination of information present in every channel and to determine the uncertainty in the final phase lag.

Table 6. Phase lags for OH/IR stars at the Galactic centre. $R_{\rm OH}$ denotes the inferred shell radius

Name	τ [days]	σ_τ	$R_{\rm OH}$ [10^{16} cm]	σ_R
OH 0.190 + 0.036	−0.4	8.1	−0.05	1.05
OH 0.071 − 0.205	17.4	14.2	2.25	1.84
OH 359.762 + 0.120	39.6	7.4	5.13	0.96
OH 359.954 − 0.041	11.6	7.0	1.50	0.91
OH 0.129 + 0.103	−6.1	21.1		
	−0.79	2.73		

Secondly systematic effects must be considered. Although the uncertainty in calibration was estimated, we should be aware that calibration inaccuracies introduce errors which correlate across the OH spectrum, i.e. all flux densities from a certain epoch are offset by the same fraction. Such systematic effects can be a serious problem because they bias the phase lag towards zero; the cross-correlation function of two "light curves" has an extra contribution at phase lag zero. We did check for such effects, but nothing significant was found.

The results on phase lags are presented in Table 6 and Fig. 6. For only one object, OH 359.762+0.120, a phase lag can be measured accurately. For OH 359.954−0.041 and OH 0.071−0.205 a phase lag is detected, but the errors are considerable. One other object, OH 0.190+0.036, has a reasonable small uncertainty in the phase lag, but the measured value seems quite small. The measurement puts an upper limit of $\approx$ 8 days on the phase lag for this object. We should treat this result with caution, because we can not fully rule out a bias.

5. Discussion

5.1. *Period distribution*

In Fig. 7 the period distribution that results from these measurements is shown, together with periods determined by Van der Veen & Habing (1993) and a sample of disk OH/IR stars (see Van Langevelde et al. 1990 for the data; the original sample is from Herman & Habing 1985a). In Herman's sample, these periods are also measured in OH. Periods by Van der Veen & Habing (1993) are measured in the infrared (see also Van der Veen & Habing 1990 and Whitelock et al. 1991). The Herman sample is defined by selecting bright 1612 MHz sources in the Galactic disk. This fact does not directly imply that the difference between the period distribution of the two samples reflects a difference in the OH/IR star population between the disk and the centre of the Galaxy. The sample of Herman may also contain weak, foreground objects, while for the Galactic centre sample it is expected that the sources are all at the same distance. Because for the current sample the surveyed area is very small we are confident that at most one or two of our objects are actually in the foreground. Indeed the OH masers with short periods in Herman's sample are mostly optically identified Miras, which would not enter the Galactic centre sample because they would generally be too faint. The lack of long periods in the sample of Galactic centre OH/IR stars, however, can not be accounted for as easily and may be an intrinsic difference between disk and centre OH/IR stars.

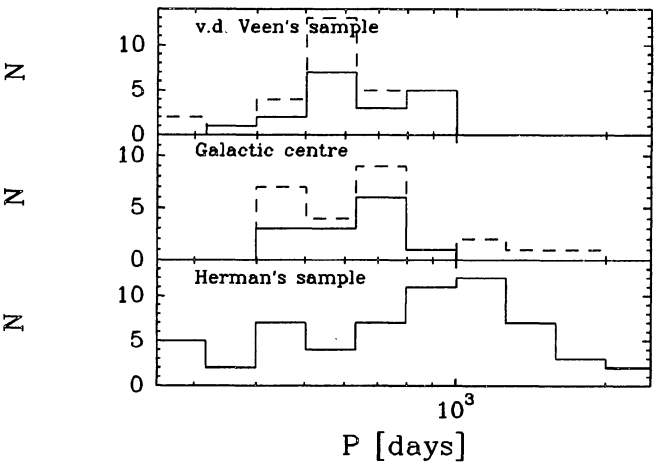

Fig. 7. Period distribution for different samples of OH/IR stars; the top panel shows periods by Van der Veen & Habing (1992), where the dashed line indicate their short period possibility for sources that had double solutions. The middle panel are results from this paper, dashed lines are sources from category 2. Bottom panel are periods from Van Langevelde et al. 1990

The comparison with the Van der Veen & Habing (1992) data is likely to be more complicated, because

this is an IR defined sample. However, the distribution of periods from that sample is almost indistinguishable from the current Galactic centre sample. Another indication that the objects in the Van der Veen & Habing (1992) sample are comparable to the stars in the current sample is that 70% out of their sample show OH maser action as well.

The overall conclusion seems to be that long period OH/IR stars are missing at the Galactic centre, in comparison with the disk of the Galaxy. This conclusion however depends somewhat on whether one wants to reject the long periods for four objects in group 2. Then the OH/IR stars at the Galactic centre appear quite similar to those in the bulge. This suggests that at the Galactic centre no massive and relatively young OH/IR stars are present. The absence of AGB stars with periods longer than 1000 days comes as a surprise; the analysis in Lindqvist et al. (1992b) seemed to suggest a population of "disk like" OH/IR stars present in the inner parts of the region. More can be said about this when we combine the data on variability with IR luminosity measurements (Blommaert et al. 1993).

5.2. *Phase lags*

The measurements of phase lags described here once again confirm the model of expanding circumstellar shells. The phase lag of OH 0.190+0.103 is quite small (< 8 days), not unlike the results for Miras by Van Langevelde et al. 1990. Although limitations in the calibration procedures can possibly bias the phase lag towards zero, we are quite convinced thet the diameter of the circumstellar shell for this object is $\leq 1\ 10^{16}$ cm. In this respect it is interesting to notice that the spectrum of OH 0.190+0.103 appears quite "filled", i.e. has quite a lot of flux at the inner velocities (Lindqvist et al. 1992a). This might be coincidence, but it can also be explained by arguing that the maser pathlengths in this source are apparently shorter, resulting in a less beamed maser profile (see Van Langevelde & Spaans 1992). According to Netzer & Knapp (1987) the shell diameter is determined by an interplay between mass-loss and interstellar UV radiation. A possible explanation for a small circumstellar shell at the Galactic centre, may be that the interstellar UV field is more powerful in this region.

6. Concluding remarks

We have been able to present parameters describing the variability of a statistically interesting sample of evolved stars that are at the Galactic centre. These data are of interest for studies concerning the stellar population at the centre of the Galaxy. Already from the period distribution of this sample there are clues that the stars that underlie the circumstellar masers in the Galactic centre differ from previously studied OH selected samples. For the brightest and most variable stars of the sample we have attempted to measure phase lags from the flux density curves, but with limited success. The accuracy of the determination of the phase lags is often dominated by calibration effects.

Acknowledgements. The authors would like to thank the AIPS group for suplying the necessary programs, especially Phil Diamond and Bill Cotton for their support when using AIPS for spectral line calibration was not standard procedure. Furthermore, the data reduction would have been impossible without the Leiden University CONVEX C-220 and the Sterrewacht workstations. We thank Walter Jaffre and Erik Deul for their help setting up and maintaining the local soft- and hardware. We acknowledge the close cooperation with Michael Lindqvist who provided us with continuous help and the positional information of the OH/IR stars prior to publication. Finally we thank Joris Blommaert for a carefull examination of the manuscript.

References

Blommaert J.A.D.L., Van Langevelde H.J., Van der Veen W.E.C.J., Habing H.J., Epchtein 1993, in preparation
Cohen R.J. 1989, Rep. Prog. Phys. 52, 881
Cornwell T.J., Perley R.A. 1992, A&A 353, 364
Cornwell T.J., Uson J.M., Haddad N. 1992, A&A 258, 583
Diamond P.J., Frail D.A., Van Langevelde H.J. 1993, in preparation
Engels D., Kreysa E., Schultz G.V., Sherwood W.A. 1983, A&A 124, 123
Habing H.J., Olnon F.M., Winnberg A., Matthews H.E., Baud B. 1983, A&A 128, 230
Herman J., Habing H.J. 1985a, A&AS 59, 523
Herman J., Habing H.J. 1985b, Physics Report 124, 255
Lindqvist M., Winnberg A., Habing H.J., Matthews H.E. 1992a, A&AS 92, 43
Lindqvist M., Habing H.J., Winnberg A. 1992b, A&A 259, 118
Netzer N., Knapp G.R. 1987, ApJ 323, 734
Thomson A.R., VLA Scientific Memorandum No. 125
Van der Veen W.E.C.J., Habing H.J. 1993, in preparation
Van der Veen W.E.C.J., Habing H.J. 1990, A&A 231, 404
Van Langevelde H.J., Cotton W.D. 1991, A&A 239, L5
Van Langevelde H.J., Diamond P.J. 1991, MNRAS 249, 7p
Van Langevelde H.J., Spaans M. 1992, in preparation
Van Langevelde H.J., Frail D.A., Cordes J.M., Diamond P.J. 1992, ApJ 396, 686
Van Langevelde H.J., Van der Heiden R., Van Schooneveld C. 1990, A&A 239, 193
Whitelock P., Feast M., Catchpole R. 1991, MNRAS 248, 276
Wood P.R. 1989, in From Miras to planetary nebulae: Which path for stellar evolution? eds. Mennessier & Omont (Editions Frontières), p. 67

Table 3. Parameters for sources in category 1. F_i denotes the equilibrium flux density in the brightest channel, 10^{a_i}, where a_i is the value of a in the channel with the highest flux density

Name	Position (1950)	$v_{*,\mathrm{LSR}}$ [km/s]	Δv [km/s]	F_i [Jy]	P [days]	σ_P [days]	b	σ_b	t_0 [-2440000]	σ_{t_0} [-2440000]	f	σ_f
OH 359.762+0.120	$17^h41^m24^s.15$ -29°03′20″.5	-5.43	29.55	5.754	757.8	6.5	0.175	0.006	5891.9	16.7	0.48	0.00
OH 0.076+0.146	17 42 03.51 -28 46 31.2	22.40	41.93	0.776	639.2	17.2	0.113	0.013	6313.8	40.9	0.48	0.02
OH 0.071+0.127	17 42 07.15 -28 47 24.7	-17.88	0.00	0.331	475.0	17.6	0.123	0.025	5594.9	76.4	0.50	0.02
OH 359.799-0.090	17 42 18.52 -29 08 05.4	-3.41	36.81	1.230	625.2	12.7	0.126	0.012	6363.6	31.3	0.57	0.01
OH 0.129+0.103	17 42 21.10 -28 45 11.3	-52.06	22.81	1.318	479.6	5.9	0.133	0.010	6063.4	18.2	0.51	0.01
OH 359.954–0.041	17 42 29.46 -28 58 37.5	70.64	40.81	3.020	781.4	10.8	0.136	0.004	6185.3	22.8	0.50	0.01
OH 359.880–0.087	17 42 29.64 -29 03 53.1	-23.65	20.43	8.128	758.8	28.0	0.038	0.003	6112.2	63.4	0.43	0.02
OH 0.060–0.018	17 42 39.36 -28 52 29.9	-3.74	39.72	0.832	470.2	7.2	0.127	0.011	5609.7	34.0	0.49	0.01
OH 0.142+0.026	17 42 40.91 -28 46 57.5	23.72	46.27	1.000	734.0	15.2	0.146	0.012	6077.8	36.0	0.50	0.01
OH 0.189+0.052	17 42 41.58 -28 43 42.3	9.90	39.65	0.759	843.2	89.4	0.127	0.019	6698.4	146.5	0.66	0.08
OH 0.190+0.036	17 42 45.48 -28 44 09.5	159.76	28.41	2.512	540.5	5.6	0.120	0.007	6346.1	15.5	0.50	0.01
OH 0.178–0.055	17 43 04.90 -28 47 40.2	-36.28	32.27	0.933	550.7	8.8	0.142	0.017	6286.9	25.1	0.51	0.01
OH 0.071–0.205	17 43 24.62 -28 57 50.9	112.71	27.31	2.089	751.8	20.6	0.138	0.008	5748.9	55.3	0.46	0.01

Table 4. Parameters for sources in category 2

Name	Position (1950)	$v_{*,\mathrm{LSR}}$ [km/s]	Δv [km/s]	F_i [Jy]	P [days]	σ_P [days]	b	σ_b	t_0 [-2440000]	σ_{t_0} [-2440000]	f	σ_f
OH 359.675+0.069	$17^h41^m23^s.55$ -29 09 22.2	-24.57	36.69	0.741	1732.7	345.0	0.170	0.034	6051.5	74.2	0.66	0.20
OH 359.974+0.16	17 41 45.10 -28 51 13.5	50.16	0.00	0.295	711.6	63.2	0.118	0.027	6135.9	134.0	0.36	0.05
OH 359.838+0.052	17 41 50.91 -29 01 36.8	-56.58	0.00	0.363	468.8	12.1	0.125	0.026	5648.8	51.0	0.51	0.02
OH 359.837+0.030	17 41 56.11 -29 02 20.6	-75.40	14.54	0.575	427.1	9.5	0.111	0.019	6279.1	31.8	0.40	0.02
OH 359.825–0.024	17 42 06.97 -29 04 41.4	-53.68	42.04	0.631	644.4	22.1	0.098	0.012	6027.6	56.8	0.50	0.02
OH 359.776–0.120	17 42 22.30 -29 10 12.6	72.29	26.05	0.617	404.3	9.1	0.125	0.022	6360.5	33.3	0.52	0.02
OH 359.939–0.052	17 42 29.91 -28 59 45.6	53.03	37.45	1.096	453.4	4.9	0.106	0.007	5644.2	23.2	0.55	0.01
OH 359.932–0.063	17 42 31.39 -29 00 27.8	-73.63	0.00	0.912	774.5	51.0	0.066	0.015	5493.0	143.4	0.47	0.03
OH 359.986–0.061	17 42 38.74 -28 57 39.9	13.24	39.90	1.175	523.4	12.8	0.059	0.007	5907.4	45.3	0.53	0.02
OH 359.977–0.087	17 42 43.60 -28 58 53.6	11.37	33.64	0.776	1069.6	24.9	0.130	0.009	5913.8	38.3	0.22	0.02
OH 359.971–0.119	17 42 50.18 -29 00 14.6	-8.53	38.67	0.525	1391.2	138.9	0.185	0.016	6690.5	61.6	0.60	0.09
OH 0.113–0.060	17 42 56.95 -28 51 07.5	88.65	34.17	0.575	1135.2	61.0	0.118	0.016	5557.0	90.3	0.52	0.04

Table 5. Sources for which no fit for P were possible (group 3)

Name	Position (1950)	$v_{*,\mathrm{LSR}}$ [km/s]	Δv [km/s]	F_i [Jy]
OH 359.899+0.222	$17^h41^m20^s.34$ -28°53′09″.6	30.65	35.10	0.759
OH 359.890+0.155	17 41 34.40 -28 55 43.6	-26.65	29.50	0.355
OH 359.755+0.061	17 41 37.09 -29 05 34.8	37.45	37.50	0.603
OH 359.952–0.036	17 42 27.90 -28 58 35.2	82.15	26.90	1.202
OH 359.946–0.047	17 42 29.90 -28 59 13.5	-27.25	39.70	0.513
OH 359.938–0.077	17 42 35.69 -29 00 36.5	-83.30	24.80	7.079
OH 0.018+0.156	17 41 52.81 -28 49 10.2	102.45	13.70	0.302
OH 0.040–0.056	17 42 45.47 -28 54 42.9	71.35	41.70	0.525
OH 0.079–0.114	17 43 04.64 -28 54 34.7	50.50	29.60	0.832
OH 0.225–0.055	17 43 11.74 -28 45 15.6	-106.45	32.90	2.512
OH 0.319–0.040	17 43 21.88 -28 39 58.2	74.75	34.90	4.898

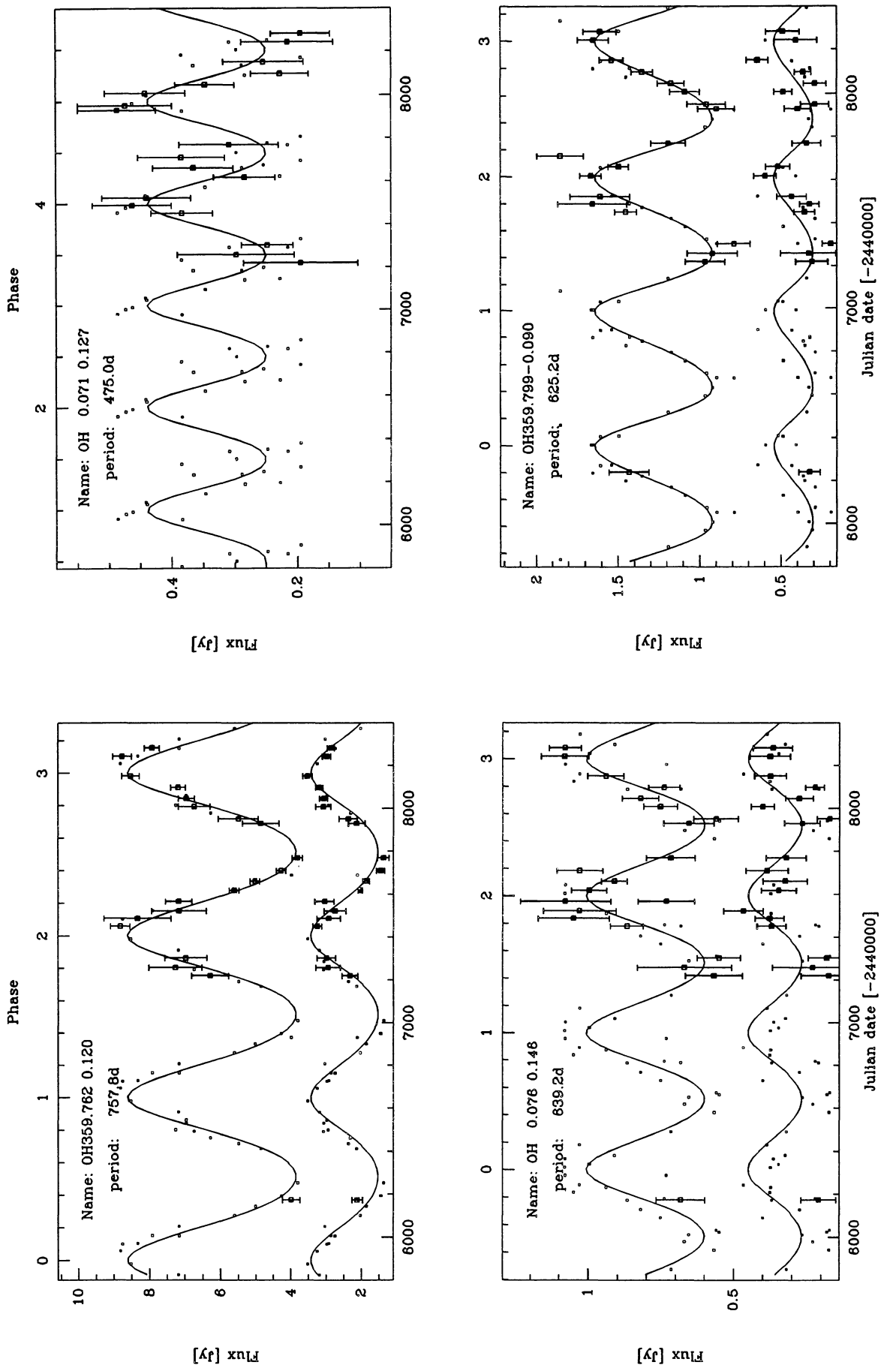

Fig. 2. Sources from category 1, unambiguous variability

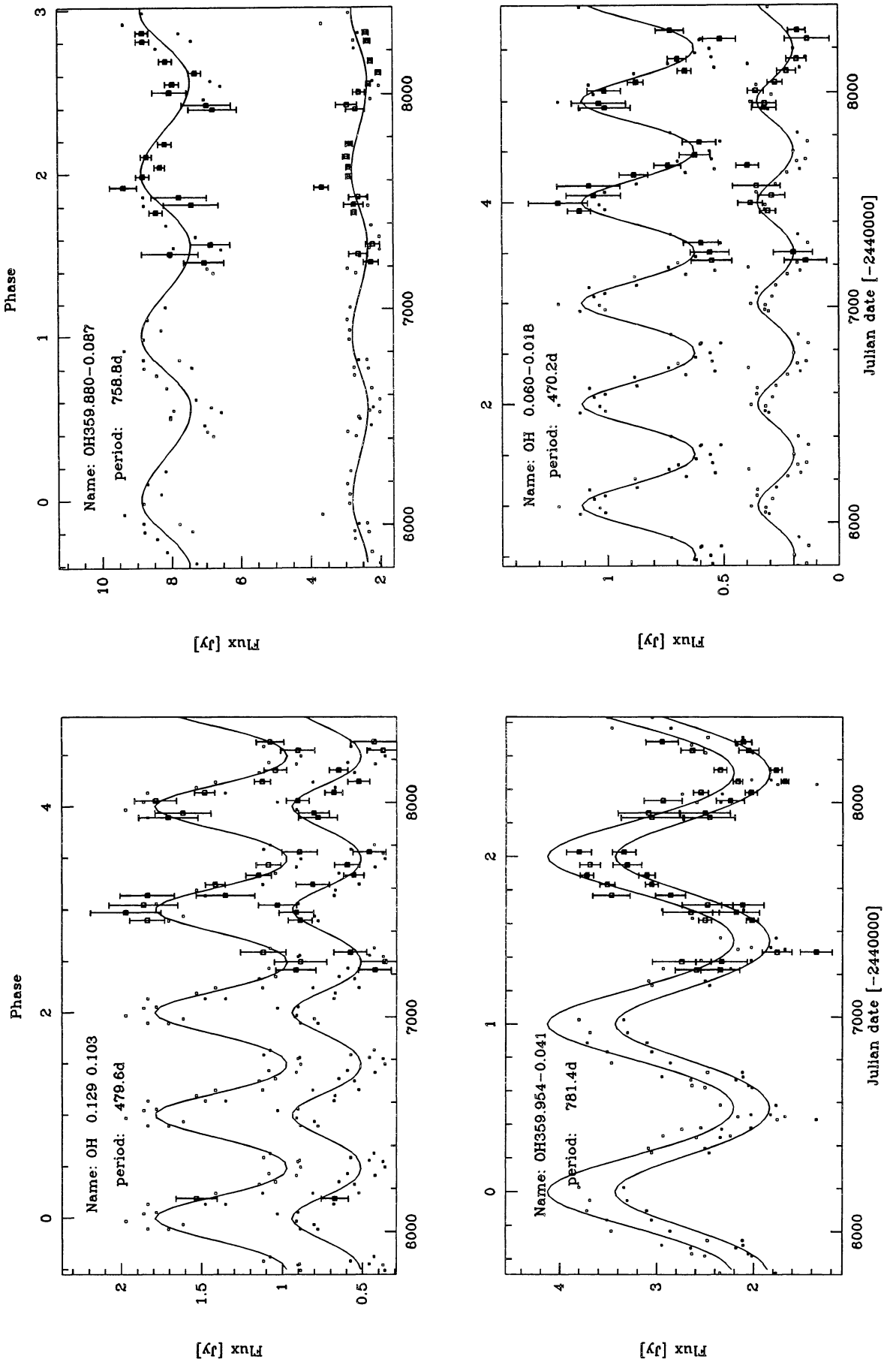

Fig. 2. continued

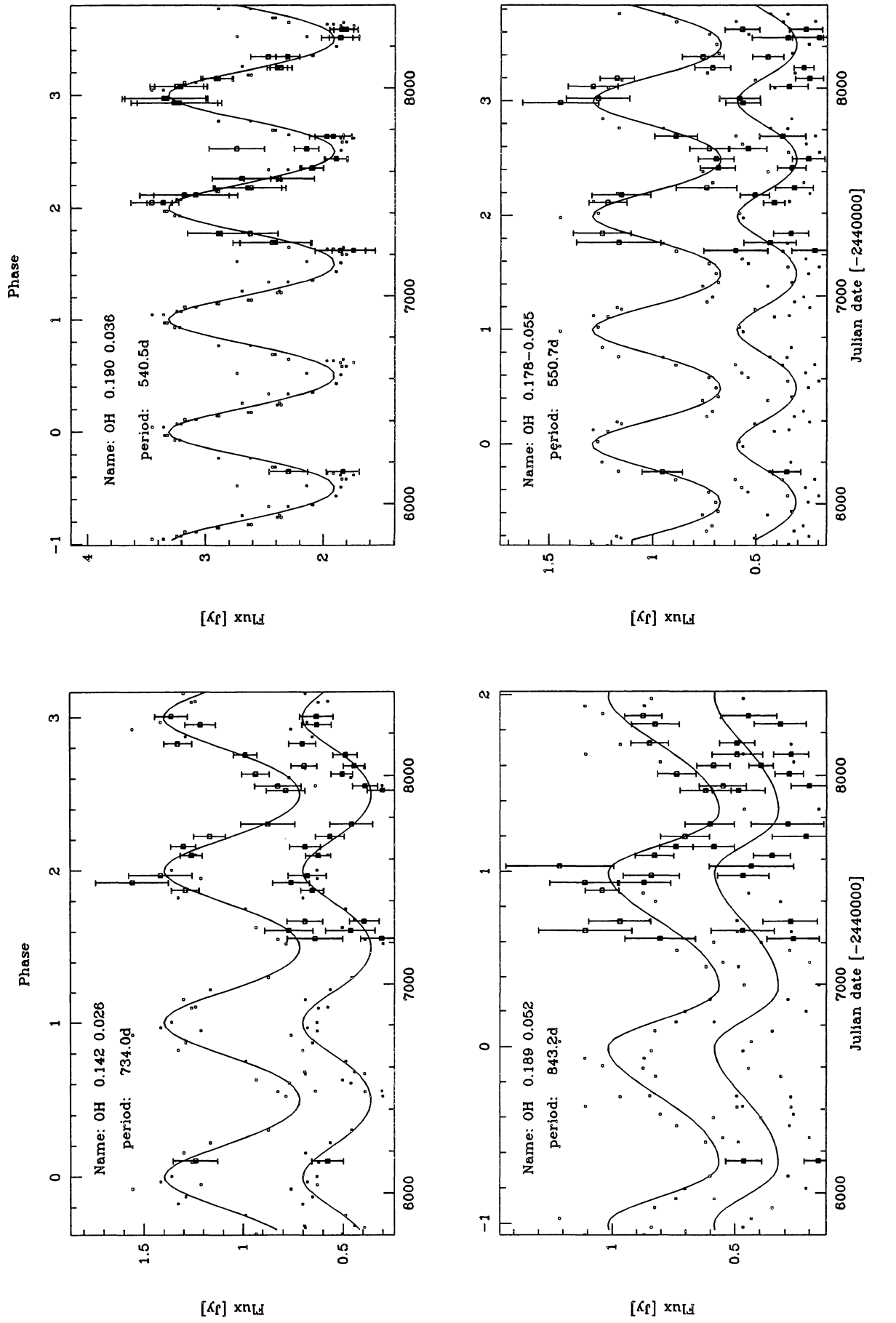

Fig. 2. continued

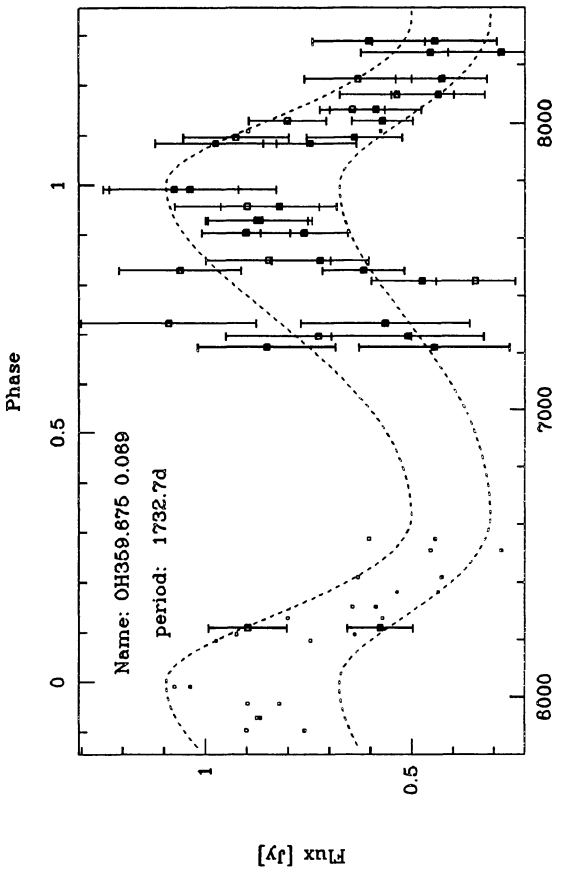

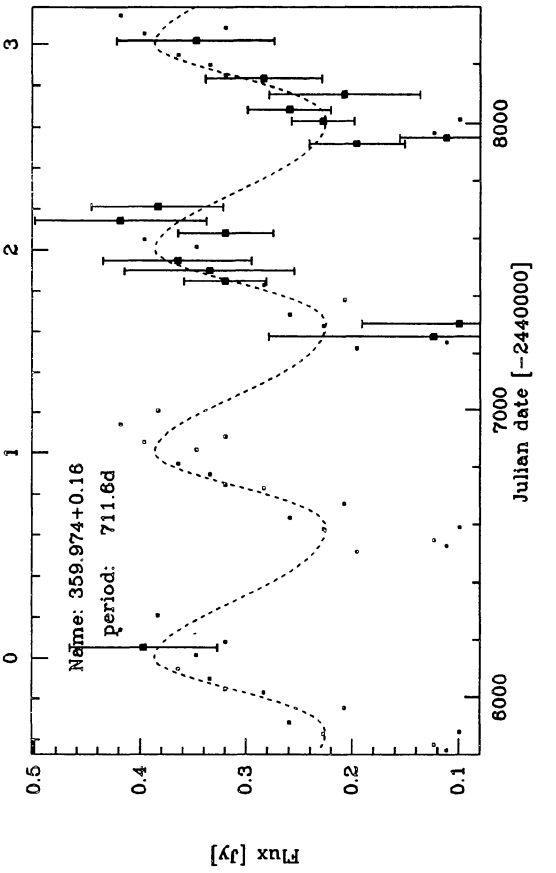

Fig. 3. Sources from category 2, possibly variable

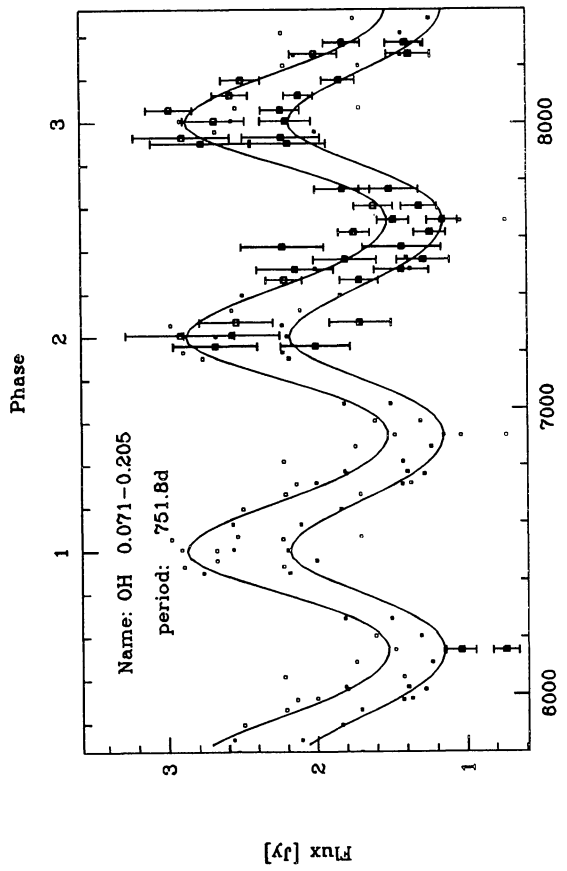

Fig. 2. continued

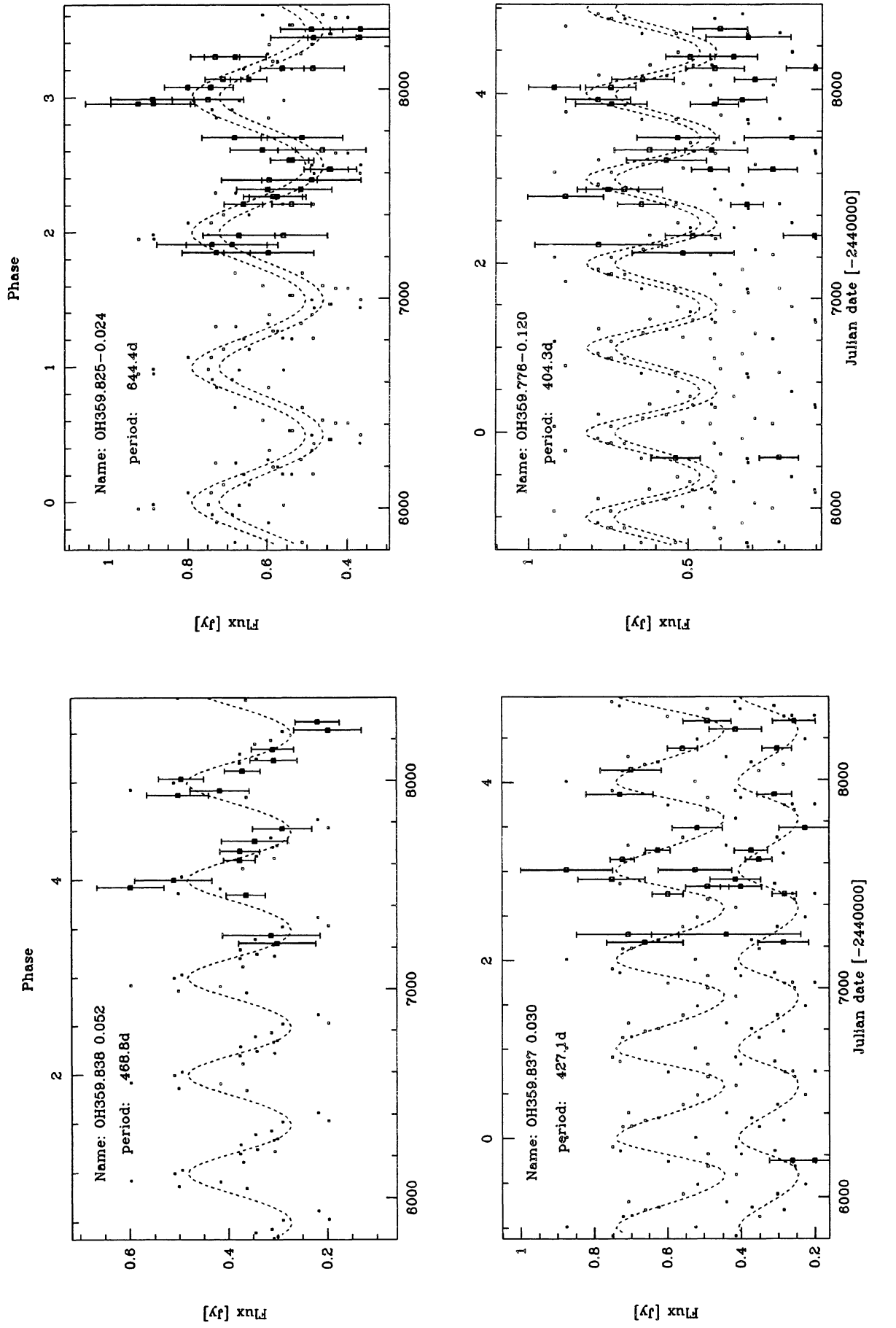

Fig. 3. continued

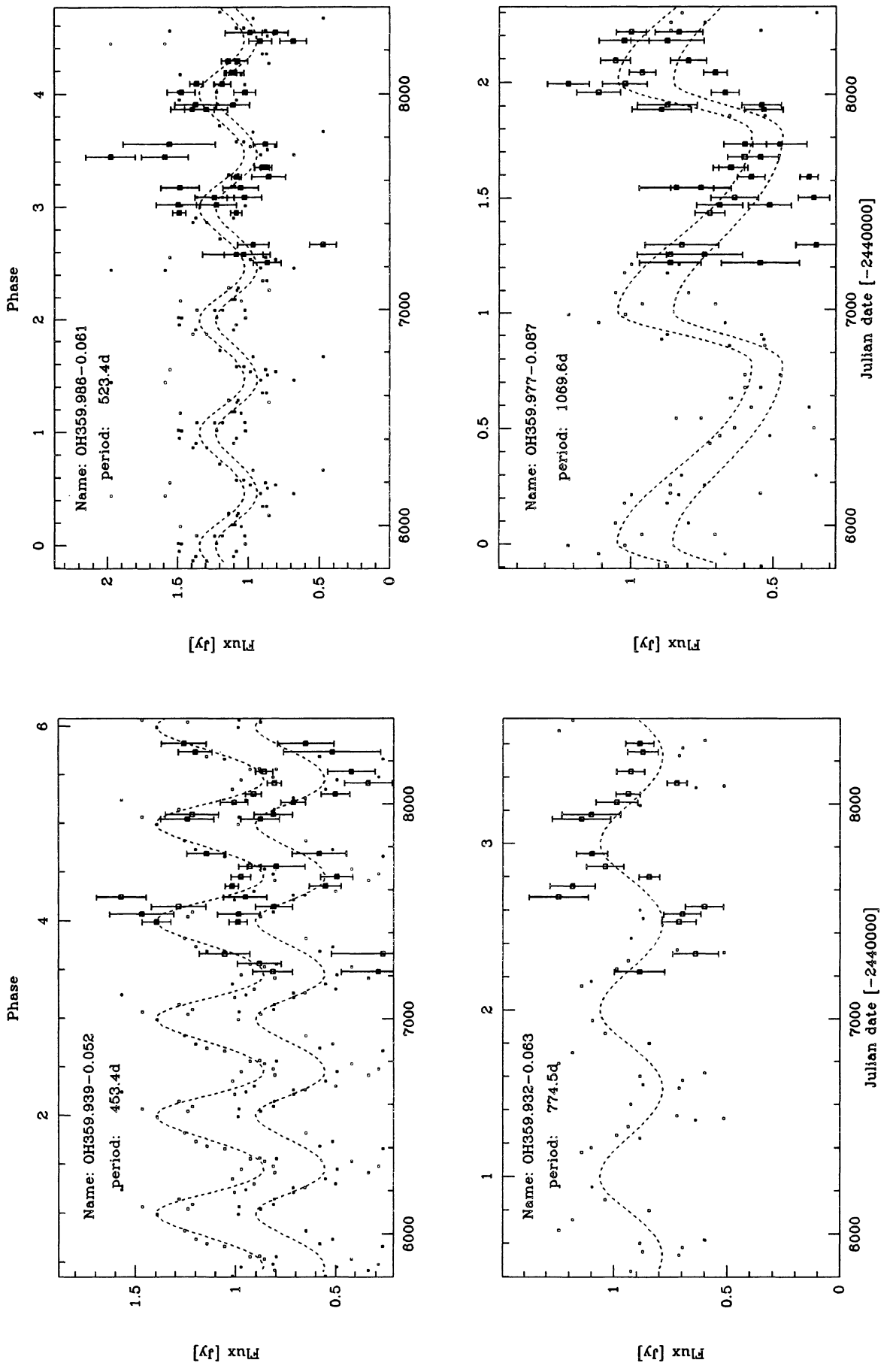

Fig. 3. continued

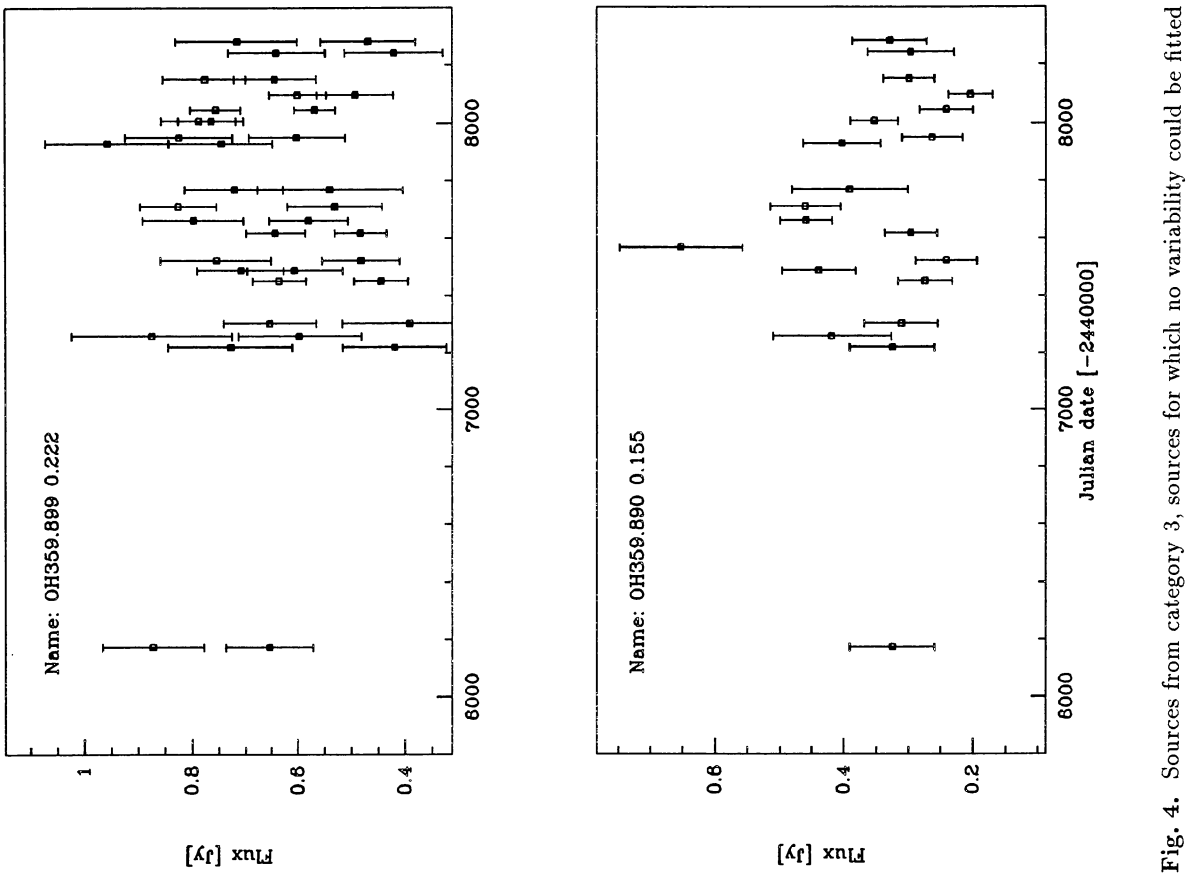

Fig. 4. Sources from category 3, sources for which no variability could be fitted

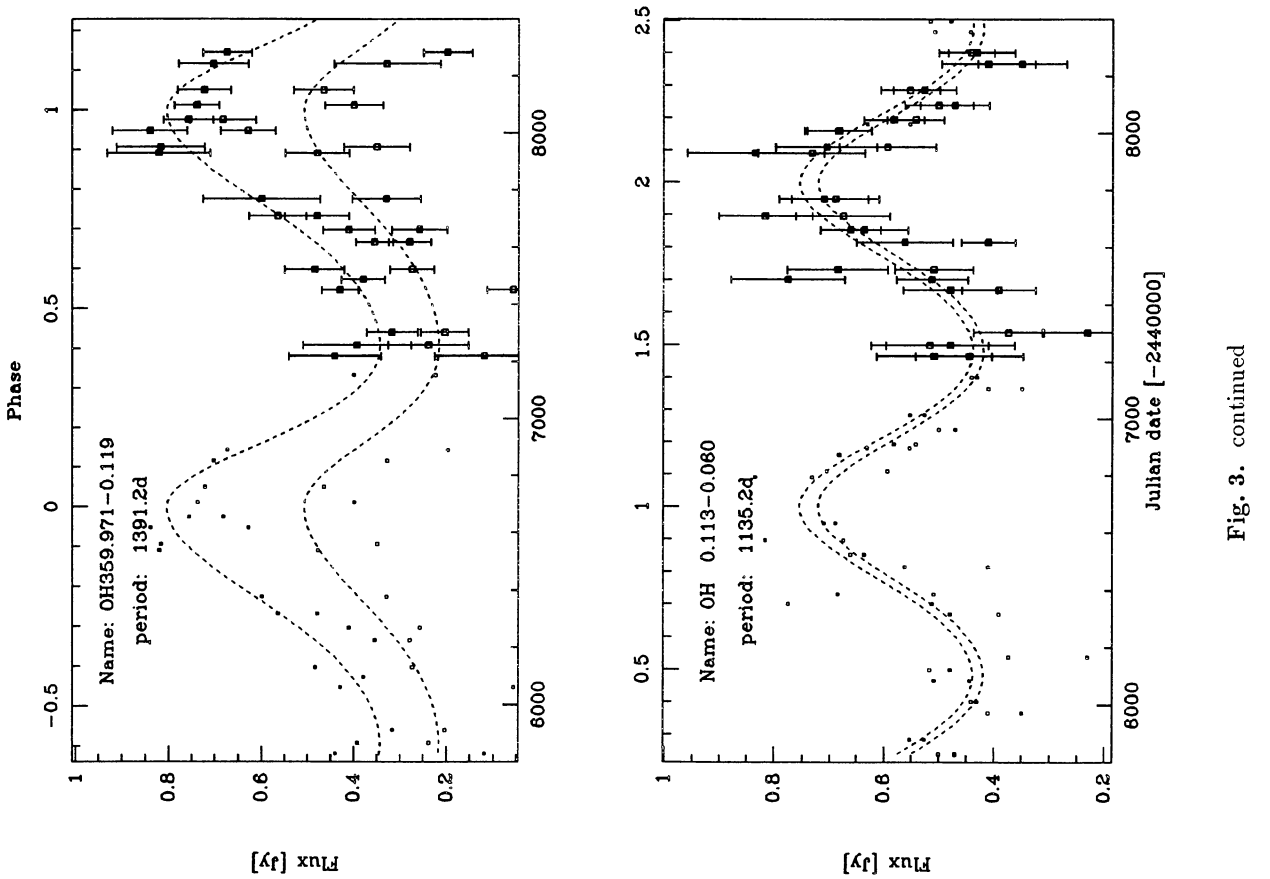

Fig. 3. continued

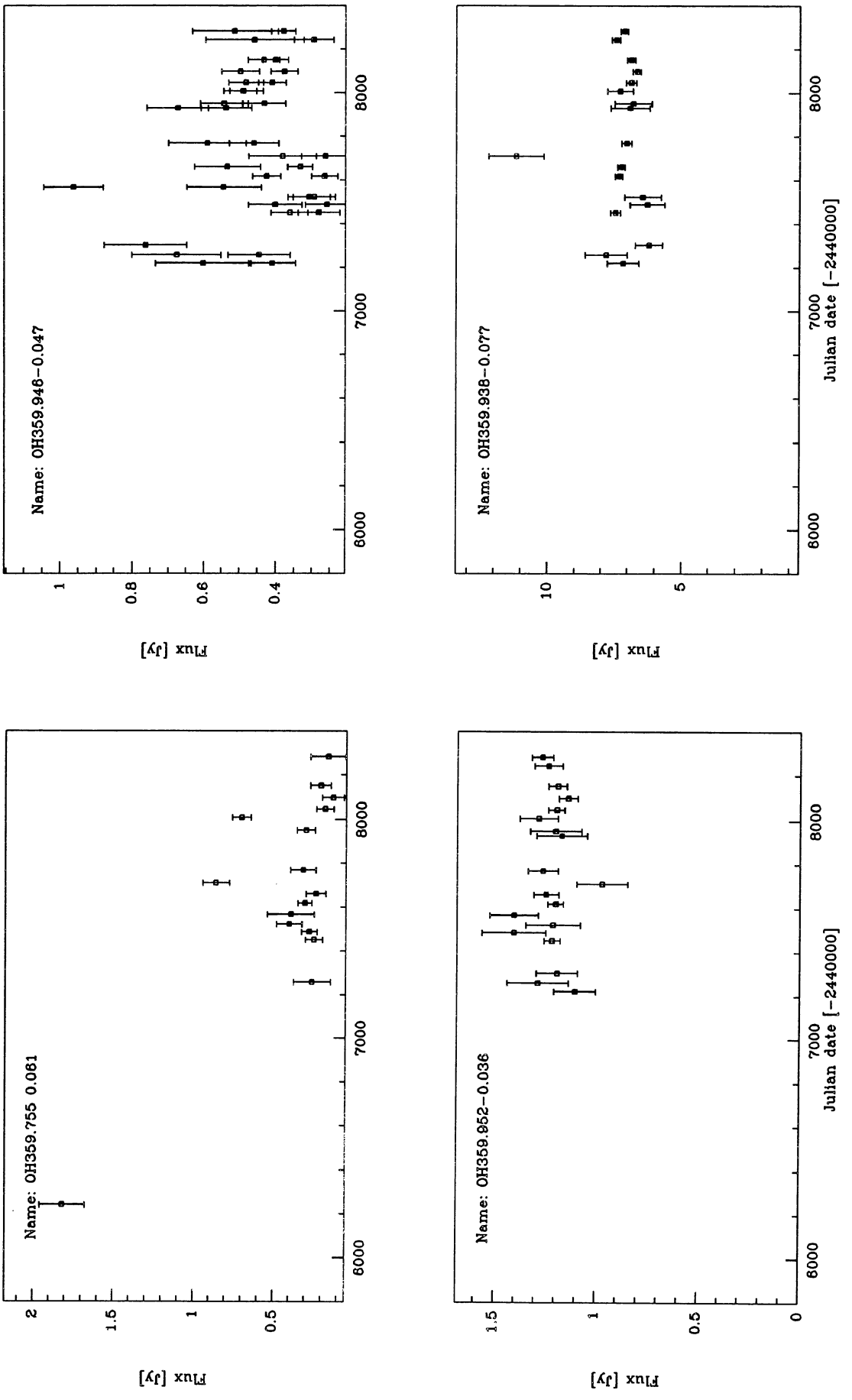

Fig. 4. continued

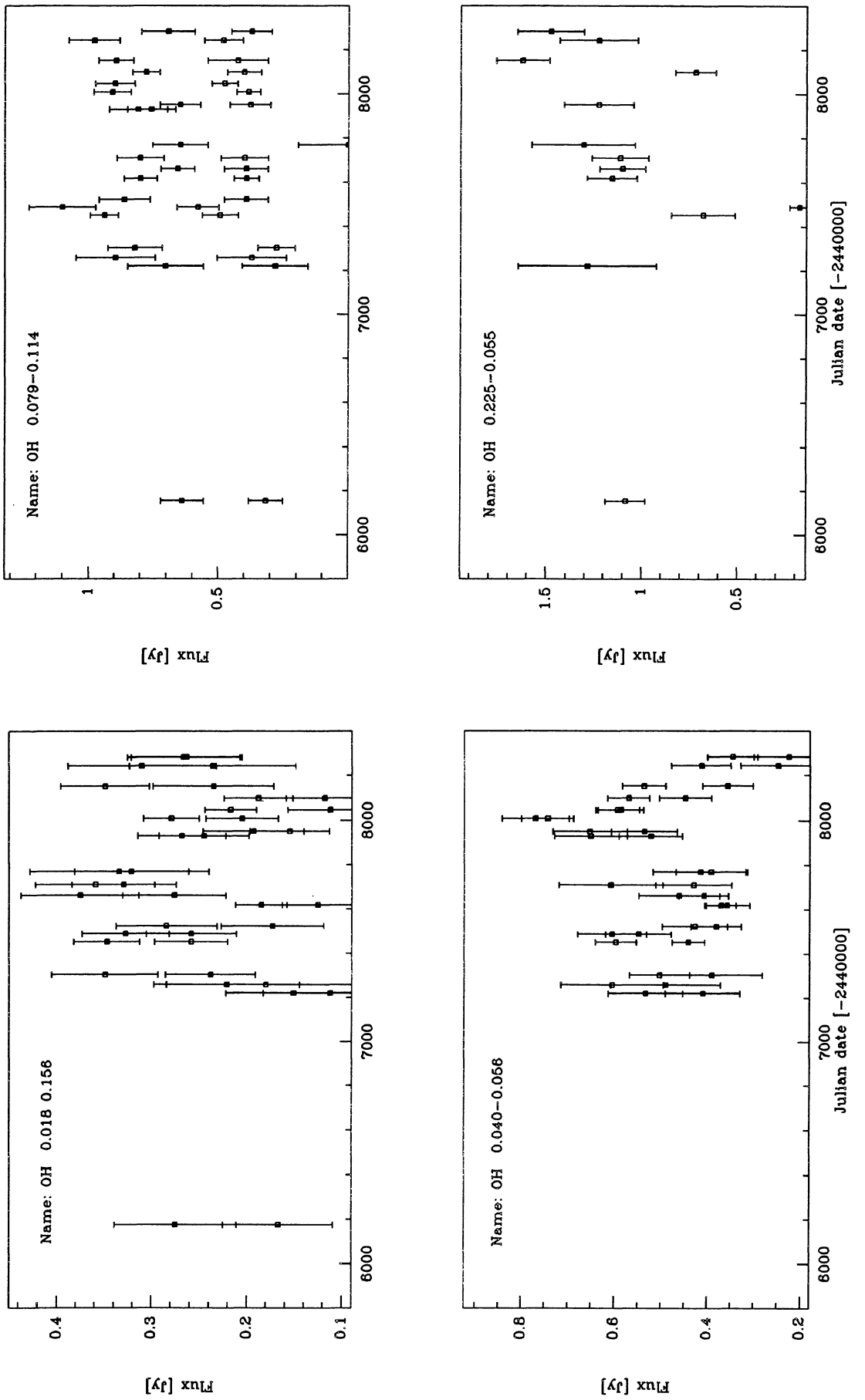

Fig. 4. continued

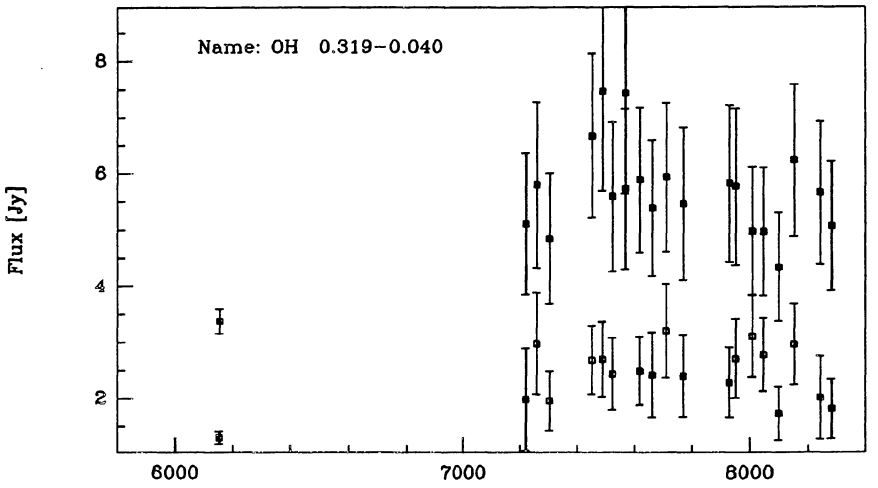

Fig. 4. continued

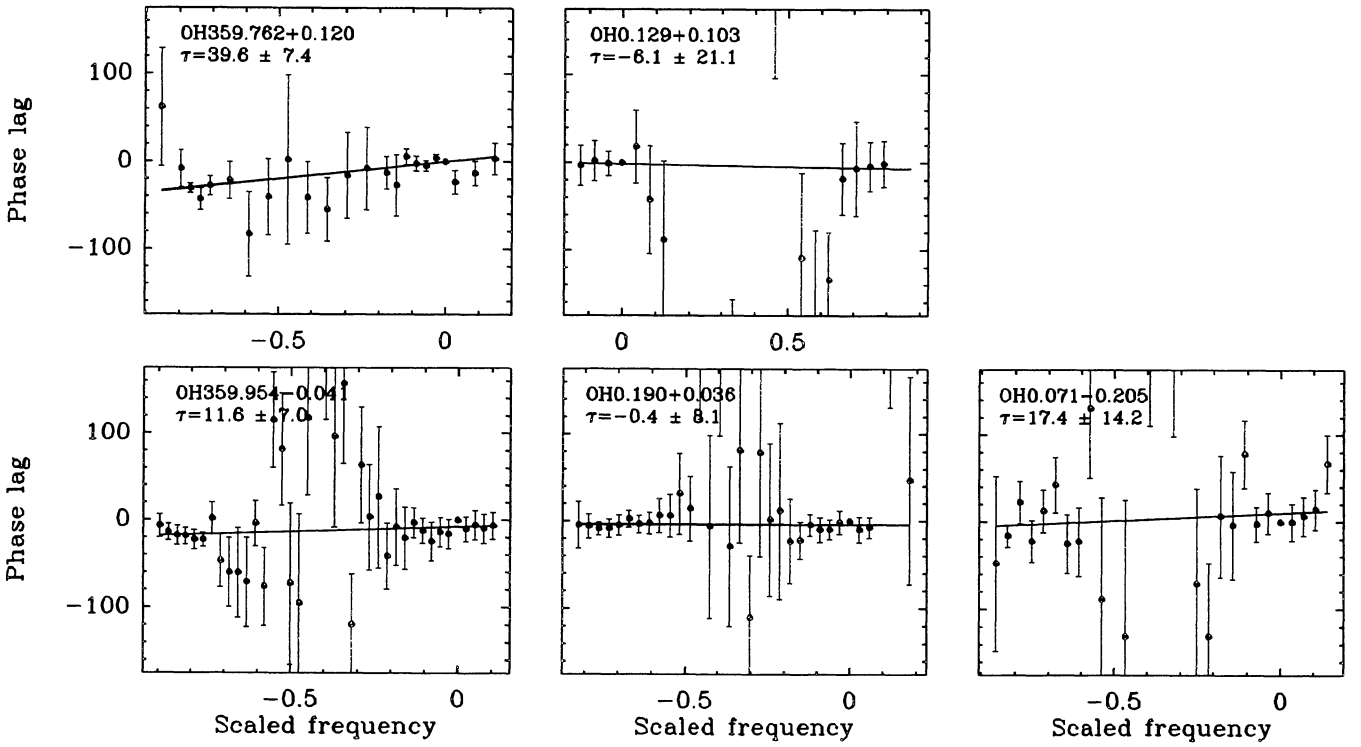

Fig. 6. Phase lags across the spectra for a subsample of five objects. The phase lag of individual channels with respect to the brightest peak are given as a function of scaled frequency, i.e. the frequency difference of a channel with the reference channel, divided by the total frequency width of the spectrum